JOURNAL OF GUIDANCE, CONTROL, AND DYNAMICS
Vol. 20, No. 3, May–June 1997

Annihilation of Transverse Velocity Bias During Spinning-Up Maneuvers

R. Anne Beck* and James M. Longuski†
Purdue University, West Lafayette, Indiana 47907-1282

During spinning-up maneuvers of a spacecraft, the spin thrusters can produce a finite transverse velocity offset or bias in the plane perpendicular to the spin axis. A two-burn scheme is introduced to eliminate this offset. The fundamental transcendental equation for the two-burn scheme is of the same form as Kepler's equation. The relationship between the transcendental equation and Kepler's equation is investigated. Numerical results demonstrate the effectiveness of the two-burn scheme.

Introduction

THE Galileo spacecraft uses a single thruster for spinup and a single thruster for spindown maneuvers. Eke and Man[1] describe the spin-rate-control flight algorithm that is used both to alter and to maintain spin rate. The problem is challenging because the thruster causes body-fixed torques about three axes and body-fixed forces along two axes.

In this paper, a maneuver scheme is presented that annihilates the transverse velocity bias accrued during spinning-up maneuvers. This offset velocity is directly dependent on the unbalanced force of the spinup thrusters and so is particularly noticeable if there is a large thruster couple mismatch or if (as in the case of the Galileo spacecraft) there is only one spinup thruster (i.e., no couple available as depicted in Fig. 1). The maneuver scheme consists of two burns with a coast period in between. The initial burn angle is given by a transcendental equation similar to Kepler's equation. However, in contrast to Kepler's equation, which has a unique solution for a given eccentricity, the transcendental velocity equation can have an infinite number of solutions. (The fact that there are close analogies between the classic problem of rigid-body motion and the orbital motion of two bodies is not new—it has been noted in an interesting paper by Cochran et al.[2])

Our problem is related to that discussed by Longuski et al.,[3] where a two-burn scheme is introduced to annihilate angular momentum bias due to transverse torques during a spinning-up maneuver. We consider the problem of transverse velocity accumulation due to transverse forces, which is not addressed in Ref. 3. Our approach makes use of the analytical approximation[4] for velocity accrued due to applied forces in a spinup maneuver. The resulting transcendental equation is different from that of Ref. 3 but is closely related. Finally, we investigate the existence of multiple solutions for the two-burn scheme.

Analytical Solutions

In this section we derive the transcendental equation for the velocity two-burn scheme. The equations of motion for a spacecraft subjected to forces and torques are highly nonlinear and difficult to analyze. However, some assumptions that simplify the dynamics, yet retain the fundamental behavior of the velocity errors, can be made.

Simple Model for Velocity Offset

We take a formal approach in the derivation of analytical solutions for the transverse velocity of a rigid body subjected to forces and torques. Let us consider Euler's equations of motion

$$\dot{\omega}_x = M_x/I_x - [(I_z - I_y)/I_x]\omega_y\omega_z \tag{1}$$

$$\dot{\omega}_y = M_y/I_y - [(I_x - I_z)/I_y]\omega_z\omega_x \tag{2}$$

$$\dot{\omega}_z = M_z/I_z - [(I_y - I_x)/I_z]\omega_x\omega_y \tag{3}$$

where M_x, M_y, and M_z are torque components; ω_x, ω_y, and ω_z are angular velocity components; and I_x, I_y, and I_z are principal moments of inertia. By assuming a near-symmetric rigid body ($I_x \approx I_y$) subjected to constant torques,[4] the spin rate is found to vary nearly linearly with time:

$$\omega_z \approx (M_z/I_z)t + \omega_{z0} \tag{4}$$

and the solutions for ω_x and ω_y can be found from Eqs. (1) and (2) in terms of Fresnel integrals. When $I_x = I_y$, the ω_z solution, Eq. (4), becomes exact.

The attitude motion of a rigid body can be expressed using a type-1 3-1-2 Euler angle sequence.[5] The corresponding kinematic equations are

$$\dot{\chi}_x = \omega_x \cos\chi_y + \omega_z \sin\chi_y \tag{5}$$

$$\dot{\chi}_y = \omega_y - (\omega_z \cos\chi_y - \omega_x \sin\chi_y)\tan\chi_x \tag{6}$$

$$\dot{\chi}_z = (\omega_z \cos\chi_y - \omega_x \sin\chi_y)\sec\chi_x \tag{7}$$

where χ_x, χ_y, and χ_z are the Eulerian angles. Equation (7), under the assumption that χ_x and χ_y are small, can be integrated analytically. The resulting solution for χ_z is

$$\chi_z \approx \tfrac{1}{2}(M_z/I_z)t^2 + \omega_{z0}t + \chi_{z0} \tag{8}$$

Without loss of generality, we may assume that

$$\chi_z(0) = \chi_{z0} = 0 \tag{9}$$

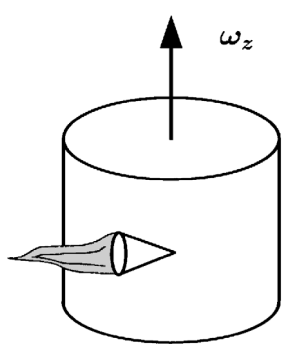

Fig. 1 Spinning-up maneuver (single thruster).

Received June 10, 1996; revision received Dec. 9, 1996; accepted for publication Dec. 31, 1996.

*Graduate Student, School of Aeronautics and Astronautics. Student Member AIAA.

†Associate Professor, School of Aeronautics and Astronautics. Associate Fellow AIAA.

This is equivalent to choosing the inertial reference frame to be coincident with the spacecraft body-fixed frame when the spinup begins.

The change in velocity in inertial space during spinning-up can be found by integrating the acceleration equations

$$\begin{bmatrix} a_X \\ a_Y \\ a_Z \end{bmatrix} = \begin{bmatrix} c\chi_z c\chi_y - s\chi_z s\chi_x s\chi_y & -s\chi_z c\chi_x & c\chi_z s\chi_y + s\chi_z s\chi_x c\chi_y \\ s\chi_z c\chi_y + c\chi_z s\chi_x s\chi_y & c\chi_z c\chi_x & s\chi_z s\chi_y - c\chi_z s\chi_x c\chi_y \\ -c\chi_x s\chi_y & s\chi_x & c\chi_x c\chi_y \end{bmatrix} \begin{bmatrix} f_x/m \\ f_y/m \\ f_z/m \end{bmatrix} \tag{10}$$

where c and s denote cos and sin, respectively; f_x, f_y, and f_z are body-fixed force components; and m is the vehicle mass. The terms f_x, f_y, and χ_z can be large during the spinning-up maneuver. On the other hand, f_z, which results from thruster misalignment, plume impingement, and wobble angle, is usually a small term. We note, however, that nonzero values of f_z result in secular velocity terms, not only along the inertial Z direction, but also in the inertial XY plane. This problem is analyzed by Beck and Longuski.[6] For the current problem we assume that $f_z = 0$. So when χ_x and χ_y are small, the transverse acceleration equations reduce to

$$\begin{bmatrix} a_X \\ a_Y \end{bmatrix} = \begin{bmatrix} \dot{v}_X \\ \dot{v}_Y \end{bmatrix} = \begin{bmatrix} c\chi_z & -s\chi_z \\ s\chi_z & c\chi_z \end{bmatrix} \begin{bmatrix} f_x/m \\ f_y/m \end{bmatrix} \tag{11}$$

Under further assumptions (corresponding to the self-excited rigid-body problem[7]) that the body-fixed forces and vehicle mass properties remain constant, the resulting linear equations can be integrated directly to obtain the transverse components of the velocity in inertial space, namely v_X and v_Y. To state the velocity solution in compact form, we define the following complex quantities:

$$a = a_X + ia_Y, \qquad v = v_X + iv_Y, \qquad f = f_x + if_y \tag{12}$$

The transverse acceleration equation then becomes

$$a = (f/m)\exp(i\chi_z) \tag{13}$$

and the corresponding transverse velocity is

$$v = v_0 + \frac{f}{m}\int_0^t \exp(i\chi_z)\,\mathrm{d}t \tag{14}$$

where $v_0 = v(0)$.

For subsequent analysis and computations, it is convenient to introduce a time-like independent variable υ and rewrite the velocity solution. We define the new independent variable υ to be

$$\upsilon(t) = \omega_z(t) = (M_z/I_z)t + \omega_{z0} \tag{15}$$

where

$$\upsilon(0) = \upsilon_0 = \omega_{z0} \tag{16}$$

Then Eq. (8) becomes

$$\chi_z(\upsilon) \approx (\lambda/2)\left(\upsilon^2 - \upsilon_0^2\right) \tag{17}$$

where

$$\lambda = I_z/M_z \tag{18}$$

The transverse velocity Eq. (14) becomes

$$v = v_0 + \frac{f}{m}\lambda\exp\left(-i\frac{\lambda}{2}\upsilon_0^2\right)\int_{\upsilon_0}^{\upsilon}\exp\left(i\frac{\lambda}{2}\upsilon^2\right)\mathrm{d}\upsilon \tag{19}$$

The integral in Eq. (19) can be written (in a way similar to that of Tsiotras and Longuski[8]) as

$$\int_{\upsilon_0}^{\upsilon}\exp\left(i\frac{\lambda}{2}\upsilon^2\right)\mathrm{d}\upsilon = \sqrt{\frac{\pi}{|\lambda|}}\left[\mathrm{sgn}(\upsilon)\,E^*\left(\sqrt{\frac{|\lambda|}{\pi}}\upsilon\right) - \mathrm{sgn}(\upsilon_0)\,E^*\left(\sqrt{\frac{|\lambda|}{\pi}}\upsilon_0\right)\right] \tag{20}$$

where $E(x)$ is the complex Fresnel integral defined as

$$E(x) \triangleq \int_0^x \exp\left(-i\frac{\pi}{2}u^2\right)\mathrm{d}u \tag{21}$$

and $E^*(x)$ in Eq. (20) represents the complex conjugate. Fresnel integrals can be approximated using the υ-method of Lanczos discussed by Boersma[9] or using asymptotic expansions, series expansions, or rational functions as in Abramowitz and Stegun.[10]

Figure 2 represents a typical transverse velocity profile during a spinning-up maneuver. The velocity vector (v_X, v_Y), starting from the origin, slowly spirals inward toward an offset (nonzero), limiting value (v_X^∞, v_Y^∞). The behavior can be analyzed by taking the first-order terms of an asymptotic expansion of the Fresnel integral appearing in the transverse velocity solution [and employing Eq. (9)] to obtain[4]

$$v_X \sim (f_x/m)\left(\omega_z^{-1}\sin\chi_z\right) - (f_y/m)\left(-\omega_z^{-1}\cos\chi_z + \omega_{z0}^{-1}\right) \tag{22}$$

$$v_Y \sim (f_x/m)\left(-\omega_z^{-1}\cos\chi_z + \omega_{z0}^{-1}\right) + (f_y/m)\left(\omega_z^{-1}\sin\chi_z\right) \tag{23}$$

For long spinup durations, the real transverse velocity components v_X and v_Y approach the finite limit:

$$v_X^\infty \triangleq \lim_{t\to\infty} v_X \sim (m\omega_{z0})^{-1}\left[-f_y + f_x\alpha + \mathcal{O}(\alpha^2)\right] \tag{24}$$

$$v_Y^\infty \triangleq \lim_{t\to\infty} v_Y \sim (m\omega_{z0})^{-1}\left[f_x + f_y\alpha + \mathcal{O}(\alpha^2)\right] \tag{25}$$

where $\alpha = \dot{\omega}_z/\omega_{z0}^2$ and where we have included, for the purpose of discussion, the second-order terms from the Fresnel integral expansion. For small values of α, that is, when the velocity spiral winds in slowly toward the limiting velocity, Eqs. (24) and (25) reduce to

$$v_X^\infty \approx -f_y/(m\omega_{z0}) \tag{26}$$

$$v_Y^\infty \approx f_x/(m\omega_{z0}) \tag{27}$$

If α is large, then the second-order expansion [Eqs. (24) and (25)] and the first-order approximation [Eqs. (26) and (27)] are both insufficient to provide an accurate solution for the velocity limit point (v_X^∞, v_Y^∞). The addition of higher-order terms will not improve the accuracy because of the nature of asymptotic expansions. In this

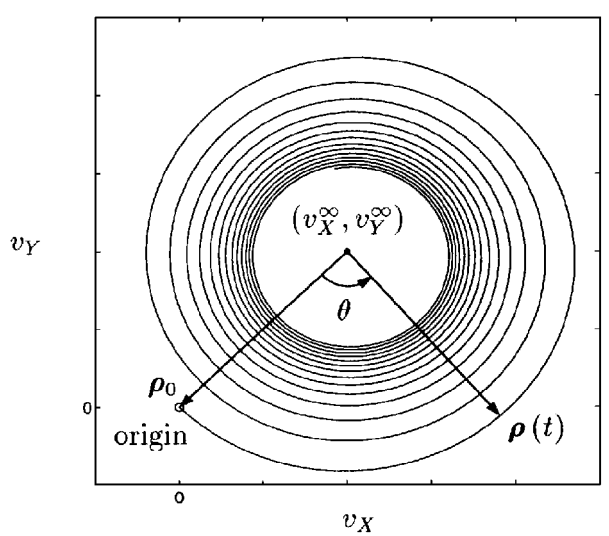

Fig. 2 Transverse velocity spiral: velocity offset $\rho(t)$.

case, we can add terms from the numerically derived Boersma expansion.[9] In any event, the concept of the two-burn scheme (which we discuss next) remains viable but may require refinement through numerical methods if α is large.

Consider now the vector $\boldsymbol{\rho}(t)$ defined with its origin at the limit point (v_X^∞, v_Y^∞) and its tip at the current position on the spinup spiral curve (as shown in Fig. 2).

That is,

$$\boldsymbol{\rho}(t) = (\Delta v_X, \Delta v_Y) \tag{28}$$

where

$$\Delta v_X = v_X - v_X^\infty, \qquad \Delta v_Y = v_Y - v_Y^\infty$$

At time $t = 0$, the vector $\boldsymbol{\rho}(0) = \boldsymbol{\rho}_0$ defines the transverse velocity offset due to the spinup maneuver. The magnitude of $\boldsymbol{\rho}(t)$ given by

$$\rho(t) = \sqrt{\Delta v_X^2 + \Delta v_Y^2} = \frac{\sqrt{f_x^2 + f_y^2}}{m\omega_z(t)} \tag{29}$$

shrinks inversely with the current spin rate, $\omega_z(t)$, spiraling inward to the limit point. We note from Eqs. (22) and (23) that θ in Fig. 2 is, in fact, the first Euler angle

$$\theta = \chi_z \tag{30}$$

To understand how the two-burn velocity scheme works, we make the following simple observations.

1) If spinning-up (thrusting) is discontinued, the motion along the velocity spiral ceases.

2) Subsequently, the vehicle continues to spin, but at a constant rate.

3) When spinning-up (thrusting) is resumed, the new velocity spiral is reoriented and has a different limit point.

In the two-burn scheme, we attempt to orient the velocity limit point of the new spiral to coincide with the origin of the velocity plane. If the velocity can be made to return to the origin, then the total accrued transverse velocity is zero.

For a slowly winding velocity spiral, it turns out that there are multiple return options in the two-burn scheme. These options occur when the perpendicular bisector between the origin and the limit point intersects the original spiral path (Fig. 3). These intersections mark locations where thrusting may be discontinued, to allow the spacecraft to rotate (coast) to a new orientation before resuming thrusting. The second burn reorients the spiral and continues its evolution in such a way as to encircle the origin.

Transcendental Equation for Burn Angle

Thus far, we have outlined a method to compute the transverse velocity and the velocity offset accrued during a spinup maneuver.

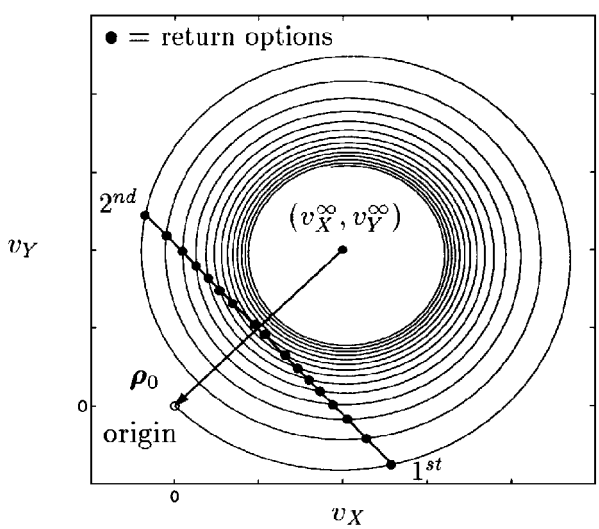

Fig. 3 Transverse velocity spiral: two-burn scheme return options.

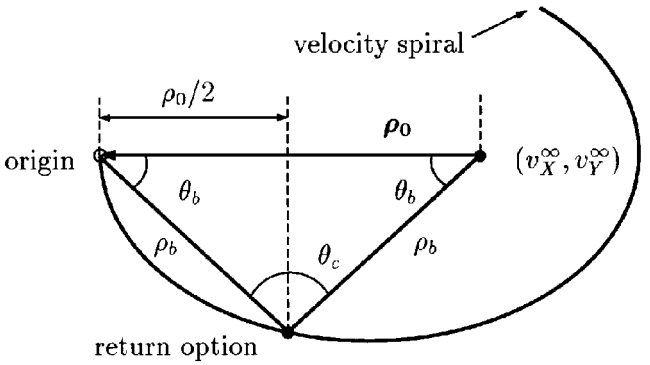

Fig. 4 Transverse velocity spiral: burn angle θ_b.

Next, we derive the governing equations for the two-burn scheme. Figure 4 illustrates the intersection of the velocity spiral with a return option. A return option establishes a switching point for the velocity two-burn scheme. The distances from this point to the origin and the limit point are equal, establishing the isosceles triangle depicted in Fig. 4.

We wish to determine the value of the burn angle θ_b. Note that in Fig. 4,

$$\rho_b \cos\theta_b = \tfrac{1}{2}\rho_0 \tag{31}$$

provides the distance between the perpendicular bisector and the origin (as well as the limit point). We can nondimensionalize the variable ρ, given by Eq. (29), as follows:

$$\tilde{\rho} = \frac{\rho(t)}{\rho_0} = \frac{\omega_{z0}}{\omega_z(t)} \tag{32}$$

At this point it is convenient to find ω_z in terms of $\chi_z\ (= \theta)$. By elimination of time in Eqs. (4) and (8), we obtain

$$\omega_z = \sqrt{2\dot{\omega}_z\chi_z + \omega_{z0}^2} = \sqrt{2\dot{\omega}_z\theta + \omega_{z0}^2} \tag{33}$$

Combining Eqs. (32) and (33), we have

$$\tilde{\rho} = \left(1 + 2\dot{\omega}_z\theta \Big/ \omega_{z0}^2\right)^{-\frac{1}{2}} \tag{34}$$

Our governing equation for θ_b, from Eqs. (31) and (32), becomes

$$\cos\theta_b = 1/2\tilde{\rho}_b \tag{35}$$

Squaring Eq. (35) and using Eq. (34), we get

$$\cos^2\theta_b = \tfrac{1}{4}\left(1 + 2\dot{\omega}_z\theta_b \Big/ \omega_{z0}^2\right) \tag{36}$$

Using the trigonometric identity, $2\cos^2\theta = 1 + \cos 2\theta$, Eq. (36) can be reduced to the transcendental velocity equation

$$1 + 2\cos 2\theta_b - \frac{2\dot{\omega}_z\theta_b}{\omega_{z0}^2} = 0 \tag{37}$$

Some remarks about Eq. (37) are in order. We first observe that ω_{z0} and $\dot{\omega}_z$ are known a priori, and hence, in principle, the burn angle θ_b can be found from Eq. (37). This defines the two-burn scheme for annihilation of velocity offset. Depending on the specific problem parameters, there may be multiple return options (as discussed earlier), which allows for greater flexibility in implementing the two-burn scheme.

Once the burn angle θ_b is found from Eq. (37), the burn time t_b is extracted from the quadratic equation [by referring to Eqs. (8), (9), and (30)]:

$$\theta_b = \left(t_b^2 \Big/ 2\lambda\right) + \omega_{z0}t_b \tag{38}$$

It now becomes necessary to define a related variable, Θ_b, as follows:

$$\Theta_b = \theta_b - 2n\pi \tag{39}$$

where n is an integer such that $0 \le \Theta_b < 2\pi$. To consider only the physically meaningful solutions, we require that Θ_b must lie in the

first or the fourth quadrant. Using the isosceles triangle in Fig. 4 and the angle Θ_b of Eq. (39), we see that the coast angle is given by

$$\theta_c = \pi - 2\Theta_b \tag{40}$$

Because the perpendicular bisector can intersect the velocity spiral twice for a given revolution, as shown in Fig. 3, there may exist a large coast angle corresponding to the second return option. The two coast angles (illustrated in Fig. 5) are given as

$$\theta_c = \begin{cases} \pi - 2\Theta_b & \text{if} \quad 0 < \Theta_b < \pi/2 \\ 5\pi - 2\Theta_b & \text{if} \quad 3\pi/2 < \Theta_b < 2\pi \end{cases} \tag{41}$$

The small angle corresponds to the return associated with the first half revolution, whereas the large angle is for the return associated with the second half revolution. Because the spin angle χ_z varies linearly with time (during coast),

$$\theta_c(t) = \omega_z(t_b)t \tag{42}$$

the corresponding coast times can be found by

$$t_c = \frac{\theta_c}{\omega_z(t_b)} \tag{43}$$

where $\omega_z(t_b)$ is the spin rate at the time when the thrusters are turned off for the coast period.

Comparison to Kepler's Problem

To show the relation between the transcendental velocity equation (37) and the well-known Kepler's equation, we define the winding parameter α and the angle Φ as

$$\alpha = \dot{\omega}_z / \omega_{z0}^2 \tag{44}$$

$$\Phi = 2\theta_b \tag{45}$$

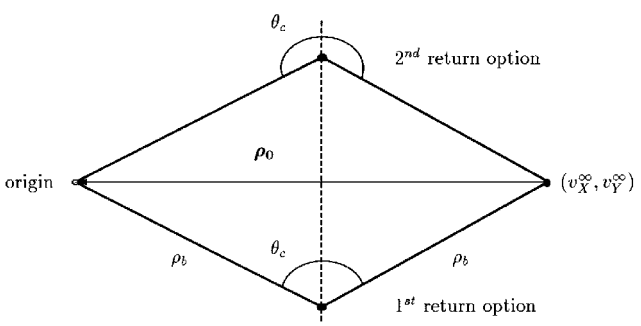

Fig. 5 Transverse velocity spiral: coast angle θ_c.

Rewriting Eq. (37) and using Eqs. (44) and (45), we obtain the transformed transcendental equation associated with the two-burn scheme:

$$\Phi - (2/\alpha)\cos\Phi = (1/\alpha) \tag{46}$$

Kepler's equation is

$$E - e\sin E = M \tag{47}$$

where E is the eccentric anomaly, e is the eccentricity, and M is the mean anomaly. The similarity between Eq. (46) and Kepler's equation is clear.

A comparison of Kepler's equation (47) and the transcendental velocity equation (46) can be drawn by considering the application of a well-known graphical solution technique, traditionally used in analyzing Kepler's equation.[11] This procedure, applied to Eq. (47), involves plotting the functions

$$y = \sin E, \qquad y = (E - M)/e \tag{48}$$

and finding the point of intersection. Because the sine curve can be constructed independently of M, only the slope and the y intercept of the straight line can vary. Figure 6 illustrates this method.

Similarly, the graphical solution for the transcendental velocity equation requires plotting

$$y = \cos\Phi, \qquad y = (\alpha\Phi - 1)/2 \tag{49}$$

and finding the points of intersection. The corresponding plot for two values of α is shown in Fig. 7. Note that, unlike Kepler's equation, the transcendental velocity equation can have multiple solutions, where each solution corresponds to a return option.

This is because the winding parameter α can take on any value ($0 \leq \alpha < \infty$), whereas the eccentricity e is limited in range ($0 \leq e < 1$). Thus, the dashed line in Fig. 6 has a slope $1/e$, which ranges between infinity and unity, whereas the dashed line in Fig. 7 can have any slope.

We see from Fig. 7 that a small spin torque (corresponding to a small winding parameter) results in a large number of points that can be considered for the two-burn return scheme. The zero-slope case, which has an infinite number of solutions, occurs when the spin rate is a constant ($\alpha = 0$). On the other hand, a large spin torque (i.e., a large winding parameter) approaches the limiting velocity at a faster rate, reducing the number of return options. One might wonder whether there are cases in which only one return option exists. Using the theory described above, this would occur for very high values of spin torque, for example a fictitious value of $M_z = 400$ N m for the Galileo spacecraft (or $\alpha = 0.9$), as shown in Fig. 7.

In general, not every solution of the transcendental Eq. (46) provides a realizable two-burn return option. We are interested only in

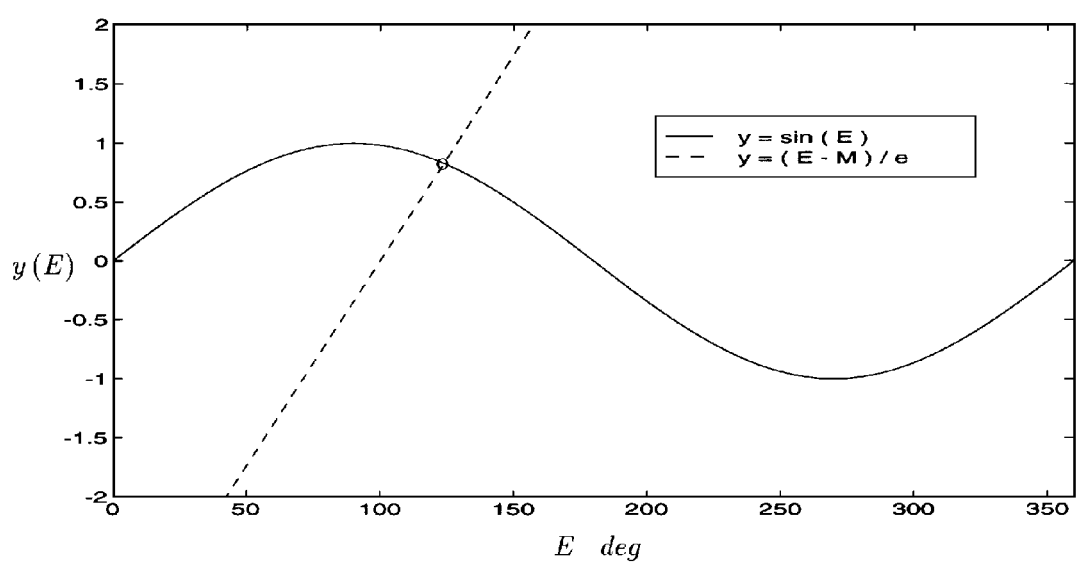

Fig. 6 Kepler relations: a simple graphical method.

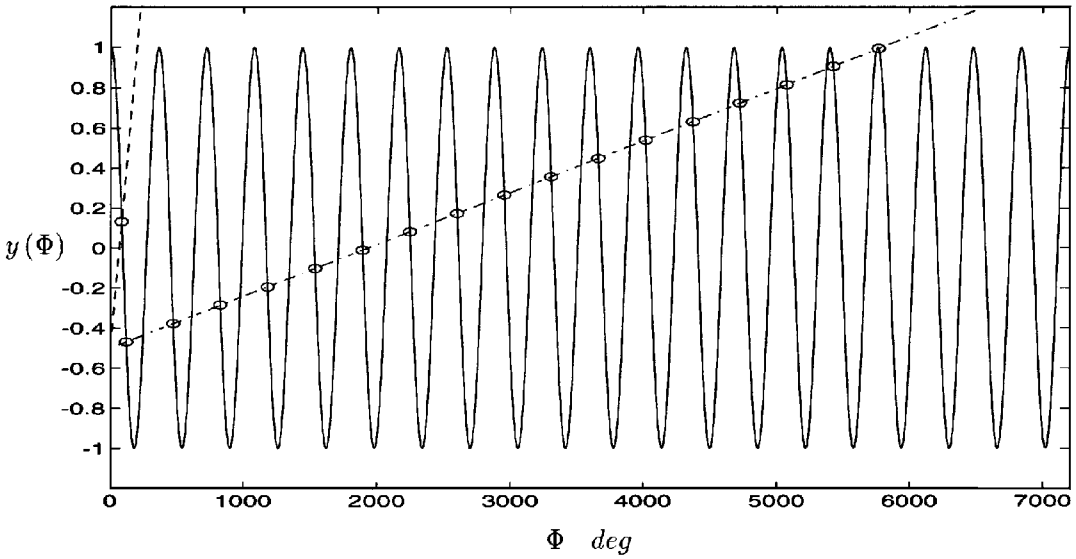

Fig. 7 Transcendental velocity relations: a simple graphical method: M_z = 400 N m (α = 0.09) and M_z = 13.5 N m (α = 0.03).

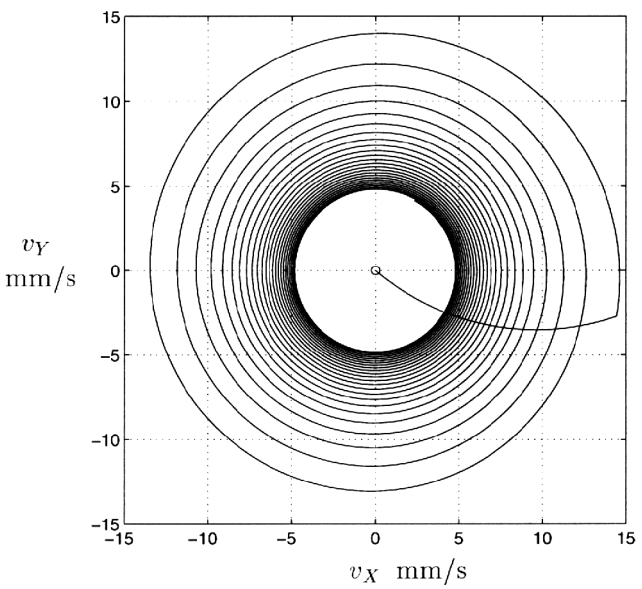

Fig. 8 Two-burn maneuver: first return option.

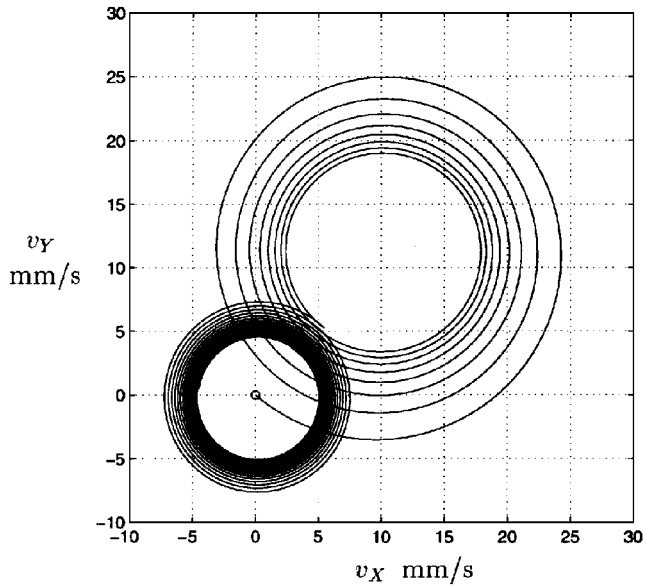

Fig. 9 Two-burn maneuver: 17th return option.

the physically meaningful solutions corresponding to the burn angles, where the related angle Θ_b lies in the interval $(0 < \Theta_b < \pi/2)$ or $(3\pi/2 < \Theta_b < 2\pi)$. It turns out that only every other intersection in Fig. 7 corresponds to a realizable return option. For the case of the Galileo, which nominally has a spin torque of $M_z = 13.5$ N m ($\alpha = 0.03$), the graphical method predicts 17 return options.

Numerical Results

It is very important to test these theoretical results as they might be applied to spacecraft maneuvers. We employ a Runge–Kutta–Verner fifth/sixth-order integration method using double-precision accuracy for the following simulations. In each case the accuracy is controlled to a tolerance of 1×10^{-10} mm/s for the velocity plots.

Axisymmetric Case

We first demonstrate the effectiveness of the two-burn scheme for an axisymmetric case. The following quantities, representative of the Galileo spacecraft,[3,7] are used in the numerical studies:

$$I_x = I_y = 2985\,\text{kg m}^2, \qquad I_z = 4183\,\text{kg m}^2, \qquad m = 2000\,\text{kg}$$

$$f_x = 7.66\,\text{N}, \qquad f_y = -6.43\,\text{N}, \qquad f_z = 0, \qquad M_x = M_y = 0,$$

$$M_z = 13.5\,\text{N m}, \qquad \omega_{z0} = 3.15\,\text{rpm}, \qquad \omega_{zf} = 10.0\,\text{rpm}$$

where we have selected axisymmetric values for I_x and I_y. This permits us to test the ideal case where Eqs. (4) and (8) are exact. We further note that the value of α is small ($\alpha = 0.03$) so that Eqs. (22) and (23) provide accurate approximations.

In the numerical simulations, for zero initial conditions on $(\omega_{x0}, \omega_{y0}, \chi_{x0}, \chi_{y0}, \chi_{z0})$, we only need to integrate the exact differential Eqs. (3), (7), and (10) to obtain the transverse velocities. From Eqs. (26) and (27) the velocity limit point is found to be $(v_X^\infty, v_Y^\infty) = (9.74, 11.6)$ mm/s. The velocity vector, for this case, spirals inward toward this limit point as expected and as shown in Fig. 2. Our objective is to cause the velocity to spiral about the origin by employing the two-burn scheme.

Figure 3 shows the 17 return options (indicated by the circles) for the case where $M_z = 13.5$ N m. Figures 8 and 9 demonstrate that the offset is returned to encircle the origin for the 1st and the 17th cases. In fact, it has been verified that the two-burn scheme reorients the velocity offset to encircle the origin in all 17 cases.

Near-Symmetric Case

In the real world, few spacecraft are axisymmetric. To study the effects of the near-symmetric case, we use the following values for I_x and I_y (Refs. 3 and 7):

$$I_x = 2985\,\text{kg m}^2, \qquad I_y = 2729\,\text{kg m}^2$$

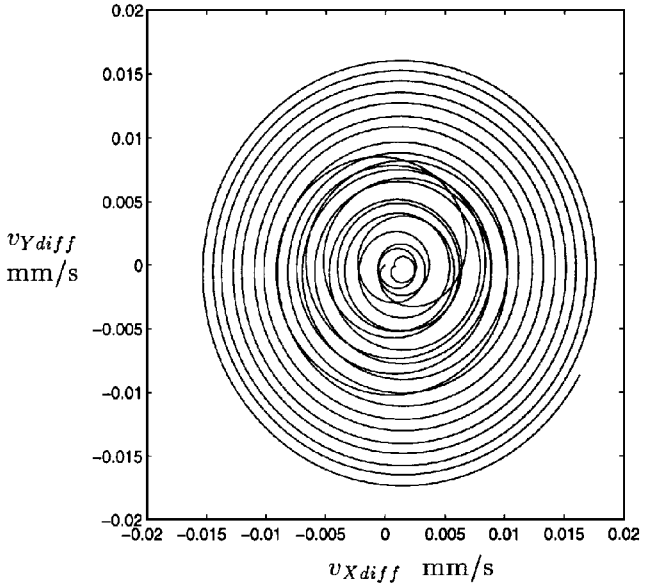

Fig. 10 Difference between near-symmetric and axisymmetric cases: first return option.

which more realistically represent the Galileo spacecraft. Of course these terms will have no effect on the validity of Eq. (4) unless both ω_x and ω_y are also nonzero, as can be seen from Eq. (3). The Galileo spacecraft has significant nonzero transverse angular velocities because of the fairly large transverse torque components produced by its single spinup thruster:

$$M_x = -1.253\,\text{N m}, \qquad M_y = -1.494\,\text{N m}$$

We now use these values in Eqs. (1–3), (5–7), and (10) to simulate the two-burn scheme, again assuming zero initial conditions for (ω_{x0}, ω_{y0}, χ_{x0}, χ_{y0}, χ_{z0}). The results are nearly identical with those of Fig. 8. To compare the two cases, we plot (in Fig. 10) the velocity differences: $v_{Y\text{diff}} = v_{Y\text{near}} - v_{Y\text{sym}}$ vs $v_{X\text{diff}} = v_{X\text{near}} - v_{X\text{sym}}$ (where the subscripts near and sym refer to the near-symmetric and axisymmetric cases, respectively). The plot shows that the maximum difference between the velocity components approaches 0.02 mm/s near the end of the maneuver. In the near-symmetric case the final values for v_X and v_Y after the maneuver are $v_{Xf} = 2.35$ mm/s and $v_{Yf} = 4.15$ mm/s as compared to $v_{Xf} = 2.28$ mm/s and $v_{Yf} = 4.19$ mm/s in the symmetric case.

These results imply that the two-burn scheme is highly practical for the more realistic case of near-symmetric spacecraft with nonzero transverse angular velocities.

Conclusions

The fundamental transcendental equation for the velocity two-burn scheme is similar to Kepler's equation but is more complicated because it has multiple solutions. This open-loop control scheme is remarkably simple to implement because it requires knowledge only of the initial spin rate and the angular acceleration to provide the burn and coast times. Major assumptions are that the thrusters can be turned on and off, that the spin torque is constant when the thrusters are on, and that the vehicle is spinning about a stable principal axis. The method applies to symmetric and near-symmetric rigid bodies.

Acknowledgments

This research is supported by Zonta International through the Amelia Earhart Fellowship, by NASA's Indiana Space Grant Consortium Fellowship, and by NASA Grant NGT-51659.

References

[1]Eke, F. O., and Man, G. K., "Galileo Spin Rate Control," AIAA Paper 82-1461, Aug. 1982.

[2]Cochran, J. E., Jr., Chang, Y.-M., and Lee, S., "Fixed-Time Reorientations of Rigid Bodies and Lambert's Problem," AAS/AIAA Astrodynamics Conf., Paper 93-582, Victoria, BC, Canada, Aug. 1993.

[3]Longuski, J. M., Kia, T., and Breckenridge, W. G., "Annihilation of Angular Momentum Bias During Thrusting and Spinning-Up Maneuvers," *Journal of Astronautical Sciences*, Vol. 37, No. 4, 1989, pp. 433–450.

[4]Hintz, G. R., and Longuski, J. M., "Error Analysis for the Delivery of a Spinning Probe to Jupiter," *Journal of Guidance, Control, and Dynamics*, Vol. 8, No. 3, 1985, pp. 384–390.

[5]Wertz, J. R. (ed.), *Spacecraft Attitude Determination and Control*, Reidel, Dordrecht, The Netherlands, 1980, pp. 763–765.

[6]Beck, R. A., and Longuski, J. M., "Analytic Solution for the Velocity of a Rigid Body During Spinning-Up Maneuvers," AIAA Paper 94-3713, Aug. 1994.

[7]Longuski, J. M., "Real Solutions for the Attitude Motion of a Self-Excited Rigid Body," *Acta Astronautica*, Vol. 25, No. 3, 1991, pp. 131–140.

[8]Tsiotras, P., and Longuski, J. M., "A Complex Analytic Solution for the Attitude Motion of a Near-Symmetric Rigid Body Under Body-Fixed Torques," *Celestial Mechanics and Dynamical Astronomy*, Vol. 51, No. 3, 1991, pp. 281–301.

[9]Boersma, J., "Computation of Fresnel Integrals," *Mathematics of Computation*, Vol. 14, 1960, p. 380.

[10]Abramowitz, M., and Stegun, I. A., *A Handbook of Mathematical Functions*, Dover, New York, 1972, pp. 297–309.

[11]Battin, R. H., *An Introduction to the Mathematics and Methods of Astrodynamics*, AIAA Education Series, AIAA, New York, 1987, pp. 192, 193.